

Quantum Dynamics of vibrationally-Assisted Electron Transfer beyond Condon approximation in the Ligand-Receptor Complex

Muhammad Waqas Haseeb¹ and Mohamad Toutounji²

¹⁾Department of Physics, United Arab Emirates University, Al Ain, UAE

²⁾Department of Chemistry, United Arab Emirates University, Al Ain, UAE

We investigate the quantum dynamics of ligand–receptor electron transfer and conformational response in a prototypical viral binding complex, using the SARS-CoV-2 Spike protein bound to the human ACE2 receptor as a model system. Treating the ACE2–Spike interface as an open quantum system embedded in a biological environment, we simulate how vibrational interactions and environmental memory reshape the coupled receptor–ligand dynamics and modulate vibrationally assisted electron transfer (VA-ET). Using a Non-Markovian Stochastic Schrödinger Equation (NMSSE) approach, we simulate electron transfer between donor and acceptor states in ACE2 that is modulated by a specific vibrational mode of the Spike protein. The influence of environmental memory (non-Markovian dynamics) and the inclusion of non-Condon effects (vibrational modulation of electronic coupling) are analyzed in detail. In the Markovian limit with an Ohmic bath, the population dynamics reduce to exponential kinetics, and the extracted transfer rates agree with semiclassical Marcus–Jortner predictions in the appropriate parameter regime. However, beyond the Markovian, high-temperature limit, we observe significant deviations: non-exponential population decay, coherent oscillatory features, and enhanced sensitivity to the vibrational mode frequency. Incorporating off-diagonal system–bath coupling (Non-Condon coupling) alongside diagonal coupling reveals that nuclear motion can dynamically gate the electron tunneling pathway, sharpening the frequency-selectivity of the VA-ET mechanism. Furthermore, a sub-Ohmic (structured) environmental spectral density, characterized by long-lived correlations (“memory”), is found to preserve electronic–vibrational coherence over longer times, thereby amplifying the vibrational selectivity of the molecular switch under the non-Condon coupling. Our results support the proposition that the ACE2–Spike interaction may exploit vibrational assistance and quantum coherence as a molecular recognition mechanism. We discuss the broader implications of these findings for understanding biological electron transfer in complex environments.

I. INTRODUCTION

Electron transfer (ET) processes lie at the heart of many biological functions, from cellular respiration and photosynthesis to enzymatic catalysis^{1–3}. Traditional theories of biological ET have been largely rooted in semiclassical formalisms such as Marcus theory and its refinements (e.g. Marcus–Jortner theory for including quantized vibrational modes), which assume rapid environmental relaxation and incoherent (exponential) kinetics^{4–6}. These frameworks have been highly successful in rationalizing reaction rates and activation energies in a variety of settings. However, a growing body of experimental and theoretical evidence suggests that many ET processes in biology can exhibit non-classical features including coherent oscillations and non-exponential kinetics especially on ultrafast timescales and in structured environments^{7,8}. For instance, ultrafast spectroscopy of photosynthetic complexes has revealed oscillatory population dynamics indicative of transient quantum coherence, challenging the notion that thermal environments immediately wash out all quantum effects in biomolecules^{9–12}. Similarly, certain enzyme-catalyzed reactions and olfactory receptor functions have been conjectured to involve quantum tunneling components beyond the classical transition-state picture^{13,14}.

One proposed quantum-mechanical mechanism of particular relevance is *vibrationally-assisted electron transfer* (VA-ET). This concept, which has roots in early ideas of

vibration-mediated processes in olfaction^{15?} ?,¹⁶, posits that a specific vibrational mode of a molecular complex can enhance or “gate” electron tunneling between two sites. In the context of olfaction, for example, it was suggested that odorant molecules with particular vibrational spectra could facilitate electron tunneling in receptors as a recognition mechanism, supplementing the usual lock-and-key binding model^{16,17}. The VA-ET mechanism essentially functions as a molecular switch tuned to a vibrational frequency: when the vibrational mode of the ligand (or another part of the complex) matches the energy requirement for electron transfer, it can resonantly assist the tunneling process, thereby turning the “switch” on¹⁸.

In this work, we explore the VA-ET paradigm in a dynamics of timely biological system: the interaction of the SARS-CoV-2 Spike protein with the angiotensin-converting enzyme 2 (ACE2) receptor on host cells. ACE2 is a metalloprotein receptor whose engagement by the viral Spike protein is the key first step for viral entry^{19–21}. Recent interdisciplinary hypotheses have proposed that, beyond the classical lock-and-key affinity of Spike for ACE2, there could be a quantum component to their binding^{22,23}. In particular, it has been speculated that electron transfer between certain residues of ACE2 (such as redox-active disulfide bonds) might be actuated by the binding of Spike, and that the Spike protein’s own dynamics possibly a specific vibrational motion could trigger this electron transfer event^{23–25}. This

is analogous to an olfactory receptor being triggered by an odorant's vibrations, but here the “odorant” is the Spike protein. Computational and experimental studies of proteins and biological recognition have indicated the critical role of specific **bond vibrational modes** in the range of 800 cm^{-1} to 1600 cm^{-1} (approximately 24 to 48 THz). These intermediate frequencies correspond to the stretching and bending of key chemical bonds (like C-C or C-N backbone motions) that possess the requisite energy to **assist electron tunneling** across the receptor-ligand interface. This energy range is thus highly relevant to our model's proposed mechanism of **vibration-assisted electron tunneling** during the SARS-CoV-2 spike protein binding to the ACE2 receptor. range^{26–28}. How can a vibration with energy smaller than typical activation energies for electron transfer substantially influence the process? One possibility is that the vibrational mode does not supply the entire energy for the electron's transition, but instead modulates the electronic coupling or alignment in the receptor to enhance tunneling probability. In other words, the vibration might act not by resonant energy donation (as a high-frequency mode could), but by dynamically tuning the pathway (a mechanism reminiscent of inelastic or “vibrational gating” of tunneling)^{29,30}.

A comprehensive theoretical treatment of such a mechanism faces several challenges. First, the biological environment (the protein matrix and membrane around ACE2 and Spike) is highly complex and structured, likely exhibiting non-Markovian dynamics. Unlike a simple solvent modeled by an Ohmic spectral density, protein and membrane environments can display slow, correlated fluctuations (e.g. $1/f$ -type noise spectra)^{31–33}. These lead to long memory times, meaning that the system's evolution at a given moment is influenced by its history over many picoseconds or longer. Standard Markovian open-system approaches (e.g. Bloch–Redfield or Lindblad master equations) fail to capture such memory effects^{34,35}. Second, the possibility of *non-Condon* effects must be addressed. The Condon approximation, typically assumed in ET theory, holds that the electronic coupling between donor and acceptor is constant (or at least independent of nuclear coordinates). In flexible biomolecular systems, this is often not true: nuclear motions can modulate the overlap of electronic wavefunctions along the tunneling path, meaning the effective tunneling matrix element becomes time-dependent. This *off-diagonal coupling* of nuclear degrees of freedom to the electronic transition (as opposed to the usual diagonal coupling that modulates site energies) can qualitatively change the ET dynamics^{29,30,36,37}. Including both diagonal and off-diagonal coupling to a bath turns the problem into a generalized spin–boson model that is not exactly solvable by simple analytic means^{38,39}. Non-Condon effects are expected to be particularly significant in the ACE2–Spike complex, given the large-scale conformational flexibility at the interface and the multiple pathways through which an electron might tunnel^{2,33}.

To tackle these challenges, we employ a non-perturbative stochastic quantum dynamics approach, namely the Non-Markovian Quantum State Diffusion (NMQSD) formalism^{40,41}. This method allows us to simulate the reduced quantum state of the system (ACE2 and the relevant Spike mode) under the influence of a realistic environment, without resorting to perturbative expansions in the system bath coupling strength. By averaging over many stochastic quantum trajectories (each representing a possible realization of the environmental noise), we obtain the ensemble dynamics equivalent to solving a non-Markovian master equation. We verify that in the appropriate limits (high temperature, fast-relaxing bath, and weak off-diagonal coupling), our approach reproduces classical Marcus–Jortner kinetics, thereby providing a consistency check^{6,42}. We then proceed to explore regimes of strong coupling, mid-frequency vibrational assistance, and structured environmental noise to uncover how these factors collectively affect the efficiency and specificity of the VA-ET mechanism in the ACE2–Spike system.

The remainder of this paper is organized as follows. In Section II, we define the system Hamiltonian and the open-system model, detailing how the vibrational mode and the environment are incorporated, including both diagonal and off-diagonal system–bath couplings. Section III outlines the theoretical foundation of the NMSSE approach and our numerical implementation, highlighting how non-Markovian environmental effects are handled via a colored-noise Stochastic Schrödinger equation. In Section IV, we present and discuss the results of our simulations. We first consider the Markovian limit with purely diagonal coupling and compare the quantum dynamics to Marcus–Jortner rate predictions. We then introduce a structured (sub-Ohmic) bath to examine non-Markovian effects on coherence and transfer efficiency. Finally, we include non-Condon (off-diagonal) coupling and demonstrate its profound impact on the vibrational gating mechanism. Section V concludes the paper with a summary of key findings, implications for the ACE2–Spike binding mechanism and similar biomolecular switches, and suggestions for future investigations, including potential experimental tests and applications in drug design.

II. THEORY AND MODEL HAMILTONIAN

A. Donor–Acceptor two-level system and vibrational mode

We model the ACE2 receptor's redox-active site as a two-level system (TLS) comprising a donor state $|D\rangle$ and an acceptor state $|A\rangle$. These could correspond, for example, to two different oxidation states or a pair of residues (such as a disulfide bond formation/breakage, or a metal ion redox couple) between which an electron can transfer when the Spike protein binds^{2,8}. The free TLS Hamilto-

nian (in two-state Pauli matrix form) is written as

$$H_{\text{TLS}} = \frac{\epsilon}{2} \sigma_z + \frac{\Delta}{2} \sigma_x , \quad (1)$$

where σ_z and σ_x are Pauli matrices in the $\{|D\rangle, |A\rangle\}$ basis. Here ϵ is the energy bias between the donor and acceptor states, and Δ is the electronic tunneling matrix element (in the absence of any vibrational or environmental interactions). In general, ϵ is related to the reaction free energy (difference in redox potentials of the donor and acceptor), and Δ sets the baseline timescale for tunneling (in absence of environment). For simplicity, we neglect any direct time-dependence of ϵ or Δ at this stage; time-dependent modulation will enter via coupling to the vibrational mode and environment.

The Spike protein is modeled as providing a single relevant vibrational degree of freedom that participates in the VA-ET mechanism. We denote this mode (for example, a hinge-bending or breathing mode of the Spike's receptor-binding domain) by a harmonic oscillator with creation and annihilation operators b^\dagger and b . Its Hamiltonian is

$$H_{\text{vib}} = \hbar\omega_v \left(b^\dagger b + \frac{1}{2} \right) , \quad (2)$$

where ω_v is the angular frequency of the mode. As noted, experimental and computational studies indicate that ω_v for Spike/ACE2 motions spans a broad range depending on the type of motion and the level of coarse-graining^{26–28}; however, in our simulations we will treat ω_v as a parameter to explore how resonance conditions affect ET. The vibrational mode is assumed to be initially in its ground state (as the Spike is not externally driven), though in a full treatment one might consider it thermally excited at physiological temperature.

The coupling between the TLS (ACE2 electronic states) and the Spike vibrational mode is a crucial part of the VA-ET mechanism. We include an interaction term of the form

$$H_{DA\text{-vib}} = \gamma \sigma_z (b + b^\dagger) , \quad (3)$$

which indicates that the occupancy of the donor vs. acceptor state (described by σ_z) is coupled to the displacement of the vibrational mode. This is a standard form of linear vibronic (Holstein/Condon) coupling and has been widely used in inelastic or vibrationally assisted ET models^{15,16}. We note that Eq. (3) is a simplifying assumption that only the energy gap is modulated by the mode; in principle, the vibrational motion could also modulate the tunneling matrix element Δ , which is captured in our model through off-diagonal (non-Condon) environmental coupling (see below). The total system Hamiltonian, combining Eqs. (1), (2), and (3), is then

$$H_{\text{sys}} = H_{\text{TLS}} + H_{\text{vib}} + H_{DA\text{-vib}} . \quad (4)$$

B. Environmental coupling: Condon (diagonal) and Non-Condon (off-diagonal)

The ACE2–Spike complex is not isolated, but immersed in a thermal environment comprised of the surrounding protein structures, lipid membrane, and solvent. We model this environment as a bath of harmonic oscillators (standard in open quantum systems)⁶,

$$H_{\text{bath}} = \sum_k \hbar\omega_k B_k^\dagger B_k , \quad (5)$$

where B_k are bosonic annihilation operators for bath mode k with frequency ω_k . The system–bath interaction Hamiltonian H_{int} is where we incorporate two distinct types of coupling:

$$H_{\text{int}} = \sigma_z \sum_k g_k^{(D)} (B_k + B_k^\dagger) + \sigma_x \sum_k g_k^{(OD)} (B_k + B_k^\dagger) . \quad (6)$$

The first term represents *diagonal (Condon) coupling*, where bath coordinates couple to σ_z and thus generate fluctuations in the donor–acceptor energy gap. This is the conventional assumption underlying the spin–boson model and, in the appropriate high-temperature/slow-tunneling limit, leads to Marcus-type ET kinetics^{6,33}.

The second term is *off-diagonal (non-Condon) coupling*, where bath coordinates couple to σ_x and thus modulate the effective tunneling channel Δ . Such terms arise naturally when structural or electrostatic fluctuations change donor–acceptor overlap or barrier properties, and have been shown to modify ET kinetics and coherence in generalized spin–boson models^{29,30,36–39}.

In a realistic biomolecular setting, the same environmental degrees of freedom can generate both diagonal and off-diagonal fluctuations. In our numerical implementation we therefore use a single bath spectral density and study the diagonal ($L \propto \sigma_z$) and off-diagonal ($L \propto \sigma_x$) channels in separate simulations for clarity.

The influence of the environment is characterized by the bath spectral density $J(\omega) = \sum_k |g_k|^2 \delta(\omega - \omega_k)$ ⁶. We consider two prototypical choices:

- **Ohmic bath with exponential cutoff:** $J(\omega) = 2\alpha\omega e^{-\omega/\omega_c}$. This Drude–Lorentz/Ohmic form is commonly used for condensed-phase environments; depending on the cutoff frequency ω_c and temperature, it can yield approximately Markovian behavior (short correlation time) or non-negligible memory effects^{6,43}.
- **Structured (Lorentzian / underdamped Brownian oscillator) bath:**

$$J(\omega) = \frac{\alpha\omega_0^2\omega}{(\omega_0^2 - \omega^2)^2 + \beta^2\omega^2} , \quad (7)$$

where ω_0 is a characteristic bath frequency and β controls the linewidth. This form represents a structured environment with nontrivial temporal correlations⁴³.

The bath correlation function $C(t)$ is obtained from the spectral density^{6,40,41}:

$$C(t) = \frac{1}{\pi} \int_0^\infty d\omega J(\omega) \left[\coth\left(\frac{\omega}{2T}\right) \cos(\omega t) - i \sin(\omega t) \right], \quad (8)$$

where T is the temperature (in energy units, with $k_B = 1$). The bath reorganization energy is

$$\lambda_{\text{bath}} = \frac{1}{\pi} \int_0^\infty d\omega \frac{J(\omega)}{\omega}, \quad (9)$$

which quantifies the energetic cost for the environment to reorganize upon an electronic-state change^{2,33}. The explicit mode produces a Holstein reorganization energy (for the coupling convention in Eq. 3) $\lambda_{\text{mode}} = \frac{2\gamma^2}{\omega_v}$, giving the total reorganization energy $\lambda_{\text{tot}} = \lambda_{\text{mode}} + \lambda_{\text{bath}}$. Electron transfer is *activationless* when the driving force matches this cost, $\epsilon = \lambda_{\text{tot}}$ ³³. We choose parameters such that λ_{tot} is of order ~ 0.1 eV, a typical scale for protein reorganization energies^{2,33}.

III. NON-MARKOVIAN STOCHASTIC SCHRÖDINGER EQUATION APPROACH

A. Non-Markovian quantum state diffusion (NMQSD) formalism

To simulate the quantum dissipative dynamics of our system (TLS + Spike mode) under the influence of the bath, we employ the NMQSD approach developed by Diósi, Gisin, and Strunz^{40,41}. In this formalism, the reduced density operator of the system $\rho(t)$ (obtained after tracing out the bath) is represented as an ensemble average of pure-state trajectories $|\psi_z(t)\rangle$ that obey a stochastic Schrödinger equation. The subscript z indicates the dependence of each trajectory on a sample of the stochastic process (noise) $z(t)$ that encapsulates the effect of the bath. The NMQSD equation can be written (in one convenient form) as:

$$\frac{d}{dt} |\psi_z(t)\rangle = \left[-\frac{i}{\hbar} H_{\text{sys}} + L z(t) - L^\dagger \int_0^t C(t-s) \frac{\delta}{\delta z^*(s)} ds \right] |\psi_z(t)\rangle, \quad (10)$$

where L is the system coupling operator defined in Eq. (3) and $C(t-s)$ is the bath correlation function (the environmental memory kernel). The noise $z(t)$ is a complex Gaussian process with zero mean, whose two-time correlation is precisely the bath correlation function:

$$\mathbb{E}[z^*(t) z(t')] = C(t-t'), \quad (11)$$

with $\mathbb{E}[\dots]$ denoting the stochastic average. For a thermal bath initially in equilibrium, $C(\tau)$ is related to the spectral density by $C(\tau) = \frac{1}{\pi} \int_0^\infty d\omega J(\omega) (\coth \frac{\hbar\omega}{2k_B T} \cos \omega\tau - i \sin \omega\tau)$. Equation (10) is an exact reformulation of the system's

reduced dynamics under the specified system-bath Hamiltonian, but it is non-Markovian due to the memory integral term involving $C(t-s)$ and the functional derivative with respect to past noise $z^*(s)$.

The physical interpretation of Eq. (10) is as follows. Each stochastic realization $|\psi_z(t)\rangle$ evolves not only under the unitary effect of H_{sys} (first term, $-iH_{\text{sys}}/\hbar$), but also under the driving of the noise $z(t)$ coupled through L (second term). The last term, involving the memory kernel, ensures that the evolution at time t is influenced by the entire prior noise history, effectively introducing dissipation and decoherence consistent with the bath's spectrum. $L^\dagger(\delta/\delta z^*)$ acting on the state is a non-Markovian extension of the usual Lindblad damping term; it subtracts the “retarded” effect of noise that has already occurred. When the bath is memoryless ($C(t-s) \propto \delta(t-s)$), this term reduces to a simple Markovian damping term proportional to $L^\dagger L$ and one recovers a stochastic Schrödinger equation equivalent to the Lindblad master equation (an approach sometimes called quantum state diffusion in its Markov form as well)^{35,44}. The NMQSD predicated on states with normalization

$$|\tilde{\psi}_z(t)\rangle = \frac{|\psi_z(t)\rangle}{\|\psi_z(t)\rangle\|} \quad (12)$$

could be achieved using the Girsanov transformation⁴⁰.

$$\begin{aligned} \frac{d}{dt} |\tilde{\psi}_z(t)\rangle &= -iH_S \tilde{\psi}_z(t) + (L - \langle L \rangle_t) |\tilde{\psi}_z(t)\rangle \tilde{z}_t - \\ &\int_0^t ds \alpha(t, s) \left\langle (L^\dagger - \langle L^\dagger \rangle_s) \hat{O}(t, s, \tilde{z}_t) - (L^\dagger - \langle L^\dagger \rangle_s) \hat{O}(t, s, \tilde{z}_t) \right\rangle \\ &|\tilde{\psi}_z(t)\rangle \quad (13) \end{aligned}$$

where O is an operator ansatz defined by the functional derivative

$$\frac{\delta}{\delta z_s^*} |\psi_{z^*}(t)\rangle = O(t, s, z^*) |\psi_{z^*}(t)\rangle, \quad (14)$$

Where \tilde{z}_t is the shifted noise,

$$\tilde{z}_t = z_t + \int_0^t ds C(t, s) \langle L^\dagger \rangle_s \quad (15)$$

and $\langle L \rangle_s = \langle \tilde{\psi}_t | L | \tilde{\psi}_t \rangle$ is the quantum average.

The (Eq. 10 or 13) is fundamental NMSSE and the perturbative treatment starts with this equation. Directly integrating (Eq. 10 or 13) is challenging because of the functional derivative term. In practice, one can employ many schemes like a hierarchy expansion known as the *hierarchy of pure states* (HOPS) method⁴⁵, equivalently, expand the memory kernel into exponentials to introduce auxiliary variables^{43,46}, perturbative expansion of the functional derivative⁴⁷. In this work, we use a variant of the perturbative expansion of the functional derivative as we used in²³ technique to solve the NMSSE for our system. Applying the formal Perturbation theory

on operator $\hat{O}(t, s, z)$ using a series expansion in powers of $(t - s)$.

$$\begin{aligned} \frac{d}{dt} |\tilde{\psi}_z(t)\rangle &= -iH_{Sys}\tilde{\psi}_t + \Delta_t(L)\tilde{\psi}_t \\ &- g_0(t)((\Delta_t(L^\dagger)L - \langle\Delta_t(L^\dagger)L\rangle_t))|\tilde{\psi}_z(t)\rangle \\ &+ ig_1(t)(\Delta_t(L^\dagger)[H, L] - \langle\Delta_t(L^\dagger)[H, L]\rangle_t)|\tilde{\psi}_t\rangle \\ &+ g_2(t)((\Delta_t(L^\dagger)[L^\dagger, L]L - \langle\Delta_t(L^\dagger)[L^\dagger, L]\rangle_t))|\tilde{\psi}_z(t)\rangle \end{aligned} \quad (16)$$

In the context of NMQSD, first-order corrections to the leading (zeroth-order) term are governed by the characteristic system frequency ω and the relaxation rate Γ . These corrections become significant when the environmental correlation time is finite yet remains shorter than the intrinsic timescales of the system, thereby validating the use of the expanded NMQSD framework. As the correlation time approaches zero, the system's dynamics converge to the Markovian limit, wherein only the zeroth-order term persists. This transition delineates the criteria under which a quantum system displays either non-Markovian or Markovian behavior.

The time-dependent coefficients $g_i(t)$ are determined by the environmental correlation function $\alpha(t, s)$:

$$g_0(t) = \int_0^t C(t, s)ds \quad (17)$$

$$g_1(t) = \int_0^t C(t, s)(t - s)ds \quad (18)$$

$$g_2(t) = \int_0^t du \int_0^s C(t, s)C(s, u)(t - s)ds \quad (19)$$

We emphasize that this method can handle strong system–bath coupling and low-temperature (high-memory) conditions, which are necessary for our investigation. Alternative exact approaches like the quasi-adiabatic path integral (QUAPI)⁴⁸ or hierarchical equations of motion (HEOM)^{43,49} could also be used to cross-check our results; these have been successful in related contexts but often become computationally heavy for long memory times. The NMQSD approach is advantageous here because it focuses computational effort on the relevant system subspace (pure states) and treats noise influences stochastically, which can be more efficient when the effective number of degrees of freedom in the system (including memory) is not too large.

B. Extraction of observables and comparison to rate theories

From an ensemble of stochastic trajectories $|\psi_z(t)\rangle$, we construct the (ensemble-averaged) density operator

$$\rho_{\text{full}}(t) = \mathbb{E}[|\psi_z(t)\rangle\langle\psi_z(t)|]. \quad (20)$$

We typically propagate $N_{\text{traj}} \sim 10^3\text{--}10^4$ trajectories (until statistical convergence is achieved) for each parameter set. Expectation values of observables are computed as

$$\langle O(t) \rangle = \text{Tr}[O \rho_{\text{full}}(t)] = \mathbb{E}[\langle \psi_z(t) | O | \psi_z(t) \rangle]. \quad (21)$$

Because our system includes an explicit vibrational mode, we obtain the reduced electronic (donor–acceptor) density matrix by tracing out the vibrational subspace, $\rho(t) = \text{Tr}_{\text{vib}}[\rho_{\text{full}}(t)]$. The donor and acceptor populations are then $P_D(t) = \langle D | \rho(t) | D \rangle = \rho_{DD}(t)$ and $P_A(t) = \langle A | \rho(t) | A \rangle = \rho_{AA}(t)$, equivalently $P_D(t) = \langle \sigma_D(t) \rangle$ and $P_A(t) = \langle \sigma_A(t) \rangle$ with $\sigma_D = |D\rangle\langle D| = \frac{1}{2}(I + \sigma_z)$ and $\sigma_A = |A\rangle\langle A| = \frac{1}{2}(I - \sigma_z)$. We initialize the electronic subsystem in the donor state and the vibrational mode in its ground state, so that $P_D(0) = 1$ and $P_A(0) = 0$. To quantify electron-transfer kinetics we define a local (instantaneous) relaxation-rate estimator $k_{\text{inst}}(t) = -\frac{d}{dt} \ln |P_D(t) - P_D(\infty)|$, where $P_D(\infty)$ is the stationary donor population, but since numerical differentiation of stochastic data is noisy, we instead extract an effective late-time rate by fitting the long-time tail to an exponential relaxation, $P_D(t) \approx P_D(\infty) + [P_D(t_0) - P_D(\infty)] \exp[-k_{\text{rel}}(t - t_0)]$ for $t \geq t_0$, with t_0 chosen after the initial transient such that the remaining window captures near-exponential tail behavior. Equivalently, we perform a linear fit of $\ln |P_D(t) - P_D(\infty)|$ versus t in the late-time window, where k_{rel} is given by the (negative) slope. For a biased two-state kinetic model with forward and backward rates (k_f, k_b) one has $k_{\text{rel}} = k_f + k_b$ and $P_D(\infty) = k_b/(k_f + k_b)$, so this procedure provides a consistent relaxation-rate measure even when $P_D(\infty) \neq 1/2$; outside the asymptotic regime (e.g., oscillatory or multi-exponential transients) we apply this fit only after the dynamics has entered a clear exponential tail.

a. Marcus–Jortner benchmark. To make contact with classical ET theory, we compare the extracted effective rate to the Marcus–Jortner (MJ) expression for a single quantized vibrational mode ω_v and a classical bath reorganization energy λ_s ⁵⁰:

$$k_{\text{MJ}} = \frac{2\pi}{\hbar} |V|^2 \frac{1}{\sqrt{4\pi\lambda_s k_B T}} \sum_{m=0}^{\infty} e^{-S} \frac{S^m}{m!} \exp\left[-\frac{(\epsilon - (\lambda_s + \lambda_v) + m\hbar\omega_v)^2}{4\lambda_s k_B T}\right], \quad (22)$$

where $V = \Delta/2$ is the electronic coupling and ϵ is the donor–acceptor bias (reaction free energy). The classical reorganization energy λ_s is obtained consistently from the bath spectral density via λ_{bath} (see Section II), and is identified with λ_s in the MJ benchmark. For the linear vibronic coupling used in Eq. (3), $H_{DA\text{-vib}} = \gamma \sigma_z (b + b^\dagger)$, the mode reorganization energy and Huang–Rhys factor are

$$\lambda_v = \frac{2\gamma^2}{\hbar\omega_v}, \quad S = \frac{\lambda_v}{\hbar\omega_v}. \quad (23)$$

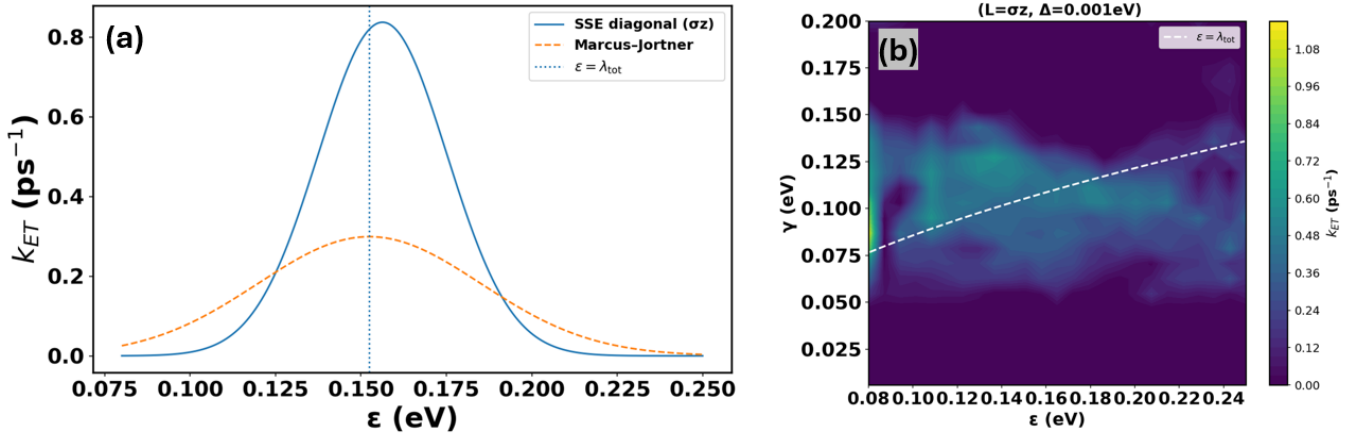


FIG. 1. **Electron-transfer rates from MSSE in the diagonal Markov regime.** Bath fluctuations are treated in the Markov limit (white-noise SSE) with diagonal system-bath coupling $L = \gamma_E \sigma_z$ (pure dephasing in the donor-acceptor basis) and an Ohmic spectral density with Drude-Lorentz cutoff. Parameters (all in eV unless noted): $\Delta = 0.001$, $\omega_v = 0.1487$, $T = 300\text{K}$; Ohmic $\alpha = 0.05$, $\omega_c = 0.5$ (bath reorganization $\lambda_{\text{bath}} = 0.0125$ eV); Linblad coupling strength $\gamma_E = 0.05$. The Spike Protein mode contributes a vibrational reorganization $\lambda_{\text{mode}} = 2\gamma^2/\omega_v$, so the total reorganization is $\lambda_{\text{tot}}(\gamma) = \lambda_{\text{bath}} + \lambda_{\text{mode}}$. (a) The rate $k_{ET}(\epsilon)$ displays a bell-shaped dependence on the driving force with a maximum near the activationless condition $\epsilon \simeq \lambda_{\text{tot}}$. The peak is relatively narrow and high because the SSE retains coherent donor-acceptor mixing and finite- Δ effects beyond the strict golden-rule limit. (b) The 2D map $k_{ET}(\epsilon, \gamma)$ shows a ridge of enhanced transfer that tracks the activationless curve $\epsilon = \lambda_{\text{bath}} + 2\gamma^2/\omega_v$ (white dashed). For small γ the bath-induced reorganization is too weak and rates remain low; for very large γ strong dressing (polaronic narrowing) and off-resonant bias suppress transfer. Between these limits, the brightest region aligns with $\epsilon \approx \lambda_{\text{tot}}(\gamma)$.

We use Eq. (22) with parameters λ_s and λ_v matched to those used in our quantum model, providing a benchmark for the incoherent (Marcus-like) regime⁵⁰.

b. Units and parameter choices. All simulations are performed at $T = 290$ K (unless stated otherwise) to mimic physiological conditions, consistent with MD studies of the SARS-CoV-2 Spike-ACE2 complex conducted near ambient temperature⁵¹⁻⁵³. We set $\hbar = 1$ internally (energies in eV for clarity) and report rates in ps^{-1} using $\hbar = 6.582 \times 10^{-4}$ eV·ps, i.e. $1 \text{ ps}^{-1} \approx 6.58 \times 10^{-4}$ eV.

The site-energy bias $\epsilon = 0.1487$ eV corresponds to an electronic gap of ~ 150 meV, occupies the same energy regime as the binding free energy ($\Delta G \simeq -0.45 \pm 0.05$ eV) inferred from atomistic MD and MM/PBSA estimates of the RBD-ACE2 interaction⁵¹, suggesting that the electronic landscape is energetically aligned with the global stability of the RBD-ACE2 complex. Furthermore, this bias falls within the activation-free Marcus-Jortner window characteristic of optimized biological electron transfer^{16,54}.

The vibronic frequency ω_v is scanned over $\omega_v \in [0.070, 0.200]$ eV ($565\text{--}1615$ cm^{-1}) to probe resonance and frequency selectivity. This window spans the experimentally observed amide and side-chain vibrational bands of the Spike S1 subunit (Amide I peak near $1650 \text{ cm}^{-1} \approx 0.205$ eV)⁵⁵⁻⁵⁷, and also overlaps the low-frequency collective modes ($\sim 0.1\text{--}3$ THz, $0.0004\text{--}0.012$ eV) reported by terahertz and GHz spectroscopy of intact virions⁵⁸, which are attributed to Spike-dominated elastic motions. A small baseline electronic coupling

$\Delta = 0.001$ eV is chosen to suppress background ET in the absence of vibronic assistance, consistent with the weak electronic overlap expected between localized donor and acceptor sites on the ACE2-Spike interface in classical MD and QM/MM analyses^{51,52}. We further explore $\Delta = 10^{-4}\text{--}10^{-1}$ eV to map the crossover from weak to strong tunneling regimes, which covers the range of couplings extracted from condensed-phase ET systems and semiempirical estimates for biological cofactors^{16,54}. The environment is parameterized through an Ohmic or structured (underdamped Brownian) spectral density with $\omega_0 \simeq 0.10\text{--}0.15$ eV, matching the experimentally resolved Spike vibrational modes and the collective frequencies used in atomistic MD correlation analyses^{51,52,58}. These choices place the model in the biologically relevant weak-to-intermediate coupling regime where vibronic assistance and environmental memory can jointly modulate electron-transfer efficiency.

IV. RESULTS AND DISCUSSION

A. Markovian dynamics and validation against Marcus-Jortner theory

We first consider the case of an Ohmic environment (Markovian limit) with purely diagonal system-bath coupling in Eq. (16)). The spectral density is chosen to be Ohmic with a high cutoff frequency (we use ω_c on the order of a few times the largest system frequency so that

environmental correlation time $\tau_c \sim 1/\omega_c$ is very short). In this regime, the NMQSD simulation should reproduce results consistent with a Redfield/Lindblad description and with classical ET rates^{6,34,35}. The figure presents the electron transfer rate k_{ET} as a function of energy bias ϵ and ACE2-Spike coupling strength γ for a Markovian system with diagonal system-bath coupling ($L = \gamma_E \sigma_z$) and an Ohmic spectral density. The simulation parameters model solvent-driven electron transfer: electronic coupling $\Delta = 0.001\text{eV}$, spike frequency $\omega = 0.1487\text{eV}$, temperature $T = 290\text{K}$, Ohmic bath coupling strength $\alpha = 0.05\text{ eV}$, Drude-Lorentz cutoff frequency $\omega_c = 0.5\text{ eV}$, and coupling operator strength $\gamma_E = 0.05\text{ eV}$. This configuration yields a bath reorganization energy $\lambda_{bath} = 0.0125\text{ eV}$, while the Spike protein mode contributes a vibrational reorganization $\lambda_{mode} = 2\gamma^2/\omega_v$, resulting in a total reorganization energy $\lambda_{tot}(\gamma) = \lambda_{mode} + \lambda_{bath}$ that varies with ACE2-spike coupling strength γ .

In the diagonal Markov limit with an Ohmic environment, the Markovain Stochastic Schrodinger (MSSE)(See Appendix A) reproduces Marcus-Jortner rates (k_{MJ}) the canonical activationless behavior of electron transfer. The rate is optimized when the energetic driving force ϵ compensates the total reorganization $\lambda_{tot} = \lambda_{bath} + 2\gamma^2/\omega_v$. **Panel(a)** shows the resulting bell-shaped $k_{ET}(\epsilon)$ at fixed γ ,while **Panel (b)** reveals a ridge of high rates that follows the activationless relation as γ is varied. According to Marcus theory, the rate as a function of ϵ should follow a Gaussian-like “inverted parabola” (Marcus parabola), peaking at $\epsilon = \lambda_{bath} + m\hbar\omega_v - \Delta G^\ddagger$ (where ΔG^\ddagger is the activationless condition, which in symmetric case is $\epsilon = \lambda_{bath} + \lambda_{mode}$). We performed a parameter scan varying ϵ while holding other parameters fixed, and for each ϵ we extracted k_{ET} from the long-time dynamics. **Figure 1(a)** shows the resulting k_{ET} vs. ϵ curve from MSSE (solid markers) superimposed on the Marcus-Jortner rate curve (solid line) calculated for the same parameters. The agreement is generally good: both curves exhibit a peak in the rate at $\epsilon \approx \lambda_{tot}$ as expected for activationless electron transfer, and then a turnover to lower rates in both the normal ($\epsilon < \lambda_{tot}$) and inverted ($\epsilon > \lambda_{tot}$) regimes. The MSSE yields slightly higher rates than Marcus-Jortner. This can be attributed to quantum effects beyond the semi-classical harmonic bath approximation of Marcus theory, and possibly to partial coherence in the early dynamics that Marcus-Jortner (being a fully incoherent theory) does not capture^{1,11}. Nonetheless, the correspondence in the normal region gives us confidence that our model and numerics are sound. The MSSE equation in this limit simplifies to include a stochastic term driving energy bias fluctuations and a dissipative term suppressing these fluctuations toward the mean value, resulting in purely diffusive dynamics along the energy bias coordinate without non-Markovian feedback mechanisms(**Appendix A2**).

Figure 1(b) also showing three distinct dynamical regimes emerge from the interplay between driving force and reorganization energy. In the normal regime ($\epsilon <$

λ_{tot}), rates increase with decreasing ϵ as the thermodynamic driving force grows, with stochastically driven thermal activation becoming more efficient. The activationless ridge ($\epsilon = \lambda_{tot}$) represents the optimal condition where the activation barrier vanishes, and the dissipative MSSE term localizes the system at this energy balance point. This is shown in the greener region that following the activationless line. In the inverted regime ($\epsilon > \lambda_{tot}$), rates decrease with increasing ϵ due to quantum suppression effects characteristic of the Marcus inverted region the darker region above the activationless line, where nuclear tunneling becomes significant.

The dependence of total reorganization energy on γ through $\lambda_{mode} = 2\gamma^2/\omega_v$ creates a curved activationless ridge in the (ϵ, γ) plane. At low γ values, $\lambda_{tot} \approx \lambda_{bath} = 0.0125\text{eV}$, positioning the activationless condition near $\epsilon = 0.0125\text{eV}$. As γ increases, the quadratic growth of λ_{mode} shifts the activationless ridge to higher ϵ values, demonstrating how Spike-Protien vibrational modes can tune the optimal driving force for electron transfer. This γ -dependence distinguishes the system from those with fixed reorganization energy and highlights the tunability of electron transfer rates through molecular design.

The result demonstrate how Markovian dynamics provide a foundational description of bath-driven electron transfer, where the balance between bath reorganization (λ_{bath}) and vibrational reorganization (λ_{baths}) controls activation barriers and transfer efficiency. This understanding has significant implications for designing molecular systems with optimized electron transfer rates, with applications in artificial photosynthesis, molecular electronics, drug design and energy conversion devices where reorganization energy engineering is crucial for performance.

B. Impact of non-Condon (off-diagonal) coupling and vibrational gating

We now include the off-diagonal system-bath coupling term to investigate the role of non-Condon effects on the ET dynamics unless stated otherwise, in this section we consider the structured (sub-Ohmic) bath for the environment, since that is the scenario where memory and vibrational effects interplay most interestingly^{29,30}.

The inclusion of off-diagonal coupling fundamentally changes the character of the stochastic dynamics. Even for the same initial conditions and noise realization, trajectories $|\psi_z(t)\rangle$ behave differently: they now experience random *fluctuations in the tunneling term* of the Hamiltonian. One immediate effect is that population transfer can occur in brief spurts or bursts when the random noise drives σ_x , rather than as a smooth exponential relaxation.

The electron transfer dynamics presented in **Figure 2(a,b,c)** reveal fundamentally distinct mechanisms arising from the interplay between system-bath coupling geometry and environmental interactions in a weak cou-

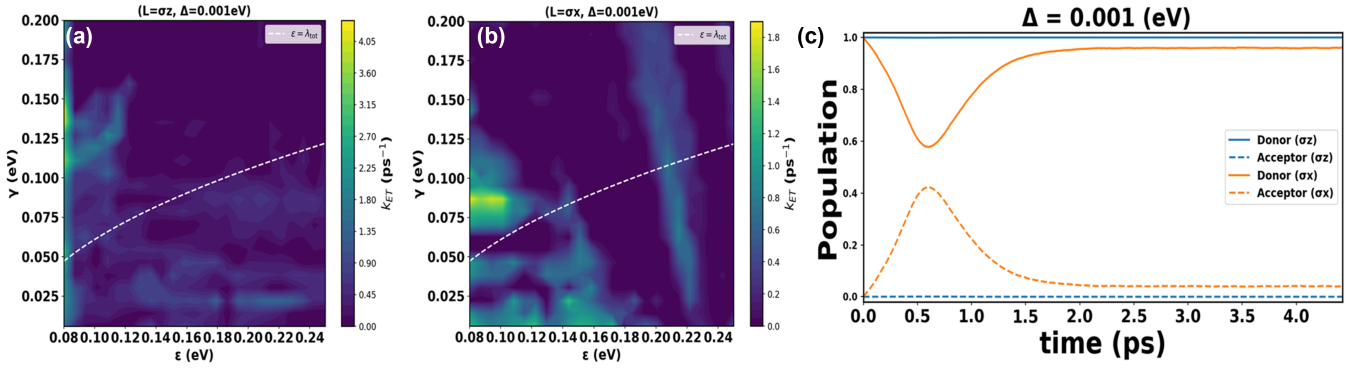


FIG. 2. Electron transfer dynamics in weak system-bath coupling regime. (a) Diagonal coupling ($L = \sigma_z$) exhibits Marcus-type behavior with activationless ridge at $\epsilon = \lambda_{tot}$ (white dashed line), where maximum rates (k_{ET}) occur due to vanishing activation energy. (b) Off-diagonal coupling ($L = \sigma_x$) shows coherent tunneling with optimal rate band ($\epsilon \approx 0.12 - 0.16$ eV, $\gamma \approx 0.05 - 0.1$ eV) deviating from activationless condition. (c) Population dynamics reveal static behavior for σ_z (blue) vs. coherent oscillations for σ_x (orange). Parameters: $\Delta = 0.001$ eV, $\alpha = 0.0005$, $\omega_0 = 0.1$ eV $\approx \omega = 0.1487$ eV, $T = 290$ K, $\gamma_E = 0.05$. NMSSE terms govern distinct mechanisms: diagonal coupling utilizes stochastic and dissipative terms for incoherent hopping, while off-diagonal coupling leverages stochastic and coherence terms for quantum tunneling. Weak coupling preserves room-temperature coherence, demonstrating quantum-to-classical transition control through system-bath geometry.

pling regime. The simulations employ parameters specifically chosen to highlight quantum effects: electronic coupling $\Delta = 0.001$ eV (weak tunneling barrier), bath coupling strength $\alpha = 0.0005$ (minimal environmental dissipation), near-resonant bath frequency $\omega_0 = 0.13 \approx \omega = 0.1487$ eV, room temperature $T = 290$ K, and bath coupling operator strength $\gamma_E = 0.05$. This parameter set creates a unique quantum-coherence-dominated environment where reorganization energy $\lambda_{bath} \ll k_B T$, decoherence times exceed and non-Markovian memory effects persist due to structured bath correlations.

Figure 2(a) illustrates the electron transfer rate k_{ET} for diagonal system-bath coupling ($L = \gamma_E \sigma_z$), exhibiting classic Marcus-type behavior with a pronounced activationless ridge. The maximum rates ($k_{ET} \approx 4.05$ ps⁻¹) align precisely with the white dashed line $\epsilon = \lambda_{tot}$, where the activation energy vanishes due to minimal reorganization energy from weak bath coupling ($\alpha = 0.0005$). The NMSSE (**Appendix A3**) terms governing this behavior include the stochastic term $\gamma_E(\sigma_z - \langle \sigma_z \rangle_t)\psi_t \tilde{z}_t$, which drives slow energy bias fluctuations enabling thermal activation over minimal barriers, and the dissipative term $g_0(t)\gamma_E^2(\langle \sigma_z \rangle_t \sigma_z - \langle \sigma_z \rangle_t^2)\psi_t$, which is extremely weak ($\gamma_E^2 = 0.0025$) and allows the system to localize at the activationless condition. The coherence term remains negligible ($\gamma_E^2 \Delta = 2.5 \times 10^{-6}$), explaining the absence of coherent transfer. Sharp transitions between normal ($\epsilon < \lambda_{tot}$) and inverted ($\epsilon > \lambda_{tot}$) regimes emerge due to minimal dissipation, while the resonant bath ($\omega_0 \approx \omega$) enhances transfer efficiency along the ridge.

In contrast, **Figure 2(b)** shows the rate map for off-diagonal coupling ($L = \gamma_E \sigma_x$), revealing coherent tunneling dynamics that deviate significantly from Marcus theory. Maximum rates ($k_{ET} \approx 1.8$ ps⁻¹) occur in a narrow band ($\epsilon \approx 0.12 - 0.16$ eV which is range for the olfactory receptor energy gap, $\gamma \approx 0.05 - 0.1$ eV) with no

alignment to the activationless line, indicating a breakdown of classical activation behavior. Here, the NMSSE (**Appendix A4**) terms operate differently: the stochastic term $\gamma_E(\sigma_x - \langle \sigma_x \rangle_t)|\tilde{\psi}_z(t)\rangle \tilde{z}_t$ directly modulates the tunneling matrix element, creating oscillatory driving forces for coherent transfer, while the weak dissipative term preserves coherence. Crucially, the coherence term $-ig_1(t)\gamma_E^2[\epsilon(\sigma_z - \langle \sigma_z \rangle_t) + 2\gamma(\sigma_z x - \langle \sigma_z x \rangle_t)]|\tilde{\psi}_z(t)\rangle$ provides significant feedback ($\gamma_E^2 \epsilon \sim 10^{-4}$) and the second that contains the non-condon effect through operator x that creates constructive interference, explaining the narrow optimal band through quantum effects. Rate suppression at low γ results from insufficient strength of ACE-Spike assistance for electron transfer, while high γ causes excessive dephasing that destroys coherence.

The population dynamics in Figure **Figure 2(c)** provide direct temporal evidence of these divergent mechanisms. For diagonal coupling (σ_z , blue lines), both donor (solid) and acceptor (dashed) populations remain static at approximately 1.0 and 0.0, respectively, throughout the simulation. This behavior arises because the NMSSE stochastic term produces only small energy fluctuations (~ 0.05 eV) insufficient to overcome the effective barrier, while the negligible coherence term offers no tunneling pathway and the weak dissipative term cannot drive relaxation. In stark contrast, off-diagonal coupling (σ_x , orange lines) exhibits pronounced coherent oscillations: the donor population decreases to 0.58 before recovering to nearly 1.0, while the acceptor population rises to 0.45 and subsequently decays. These oscillations, result from the stochastic term directly modulating the tunneling barrier, the coherence term providing phase-stabilizing feedback through ACE-spike coupling mechanism, and minimal dissipation preserving quantum superposition. The weak electronic coupling ($\Delta = 0.0001$ eV) creates a high tunneling barrier but, combined with the resonant vibra-

tional mode, enables sustained oscillations without significant energy loss.

Collectively, this **Figure 2(a,b,c)** demonstrate how system-bath coupling geometry controls the quantum-to-classical transition in electron transfer through distinct NMSSE terms contributions. Diagonal coupling (σ_z) leverages stochastic and dissipative terms to facilitate incoherent hopping, with maximum rates at the activationless condition where thermal activation barriers vanish. Off-diagonal coupling (σ_x) utilizes stochastic and coherence terms to enable coherent tunneling, where optimal rates emerge from quantum interference rather than thermal activation. The weak coupling regime amplifies these quantum effects, allowing room-temperature coherence to persist and revealing fundamental insights for biological systems (e.g., photosynthetic complexes) and quantum devices where engineered weak coupling preserves quantum coherence for efficient energy transfer^{59–61}. This analysis underscores the NMSSE as a powerful framework for unifying our understanding of electron transfer mechanisms across the quantum-to-classical spectrum.

C. Population dynamics of non-Condon (off-diagonal) coupling

We set up two comparative simulations: one with an Ohmic bath and one with a sub-Ohmic bath.

Figure 3 isolates how *geometry* (L) and *electronic coupling* (Δ) sculpt population dynamics when the bath has finite memory but very small reorganization ($\lambda_{\text{bath}} \ll k_B T$).

For $\mathbf{L} = \gamma_{\mathbf{E}} \sigma_{\mathbf{z}}$ (pure dephasing) and small Δ [panels (a)–(b)], donor and acceptor populations remain essentially fixed—dephasing randomizes phases without opening a population-transfer channel. As Δ increases [panels (c)–(d)], Hamiltonian mixing alone is strong enough to produce short-lived oscillations even under σ_z coupling, but the non-Markovian Ohmic bath rapidly damps them, yielding a monotonic approach to a donor-dominated steady state.

For $\mathbf{L} = \gamma_{\mathbf{E}} \sigma_{\mathbf{x}}$ (non-Condon/off-diagonal coupling), the bath directly modulates the tunneling pathway. Even at the smallest Δ [panel (a)], the system undertakes a coherent swing—population rises on the acceptor, then relaxes back as memory-induced damping acts. Increasing Δ [panels (b)–(d)] shortens the oscillation period and increases the initial transfer amplitude, consistent with a larger effective Rabi frequency; nonetheless, finite-temperature memory in the Ohmic kernel damps coherence on sub-ps to ps scales, driving both geometries toward similar late-time populations.

In the NMSSE, the system state $|\psi_t\rangle$ evolves under the Hamiltonian plus *colored* stochastic driving with $\langle z_t z_s^* \rangle =$

$C(t-s)$ and *memory* (time-nonlocal) feedback terms:

$$\underbrace{g_0(t) \gamma_E^2 (\langle L \rangle_t L - \langle L \rangle_t^2)}_{\text{dissipative localization}} + \underbrace{g_1(t) \gamma_E^2 C[H_{\text{sys}}, L]}_{\text{coherence feedback}}$$

(i) For $\mathbf{L} = \gamma_{\mathbf{E}} \sigma_{\mathbf{z}}$ (pure dephasing in the diabatic basis), the stochastic term produces bias fluctuations while the g_0 -term *localizes* populations; the g_1 coherence-feedback pathway is negligible because $[\sigma_z, H_{\text{sys}}] \propto \Delta \sigma_y$ is tiny at small Δ . Hence panels (a)–(b) look static, and only when Δ becomes large [panel (d)] does Hamiltonian mixing overcome dephasing to produce visible, yet rapidly damped, oscillations. (ii) For $\mathbf{L} = \gamma_{\mathbf{E}} \sigma_{\mathbf{x}}$ (off-diagonal/non-Condon), the noise $\propto (\sigma_x - \langle \sigma_x \rangle_t) \tilde{z}_t$ *directly modulates the tunneling channel*, and the g_1 term now couples strongly because $[\sigma_x, H_{\text{sys}}] \propto \epsilon \sigma_y$. This drives coherent population exchange at early times (the orange swings in all panels), after which the g_0 kernel damps the motion on sub-ps to ps scales. Increasing Δ raises the effective Rabi frequency, shortening the oscillation period from (a)–(d), while finite memory (set by ω_c^{-1}) controls the damping envelope.

Why the Ohmic case still shows coherence.? Even with an Ohmic spectrum, we do *not* take the white-noise (Markov) limit: $C(t)$ decays over a finite correlation time $\tau_c \sim \omega_c^{-1}$. This finite memory is exactly what enables the small but clear early-time oscillations in Fig. 3 (especially for $L = \sigma_x$), which would be largely washed out by a Lindblad/MSSE treatment. The small coupling α keeps $\lambda_{\text{bath}} = 1.25 \times 10^{-4} \text{ eV} \ll k_B T$, so memory—rather than strong dissipation—sets the transient coherence, while long-time behavior is governed by the dissipative g_0 kernel, yielding the damped approach to the quasi-steady populations seen across panels (a)–(d). (i) With λ_{bath} tiny, geometry—not bath strength—controls whether dynamics are *coherence-enabled* (σ_x) or *dephasing-dominated* (σ_z). (ii) Growing Δ moves the system from nearly static populations to pronounced but transient oscillations, demonstrating the crossover from incoherent (bias-localized) to coherence-assisted dynamics even in an Ohmic environment when bath memory is finite. (iii) The observed damping envelopes reflect non-Markovian friction: short-time oscillations survive long enough to reshape early dynamics but are quenched before $t \sim$ few ps at 290 K.

These results complement Figs. 1–2: there, activationless alignment explains *where* rates are large; here, Fig. 3 shows *how* populations evolve in time across Δ , clarifying the distinct dynamical fingerprints of σ_z vs σ_x coupling under the same weak, finite-memory Ohmic bath.

The Fig. 4(a-d) shows Population dynamics with a structured non-Markovian bath. Just like Figs. 3 both figures use the non-Markovian stochastic Schrödinger equation (**Appendix A3,A4**), but differ in environmental memory: Fig. 3 uses an Ohmic Drude–Lorentz spectrum with *short*, monotonic memory, whereas Fig. 4 employs a *structured* underdamped Brownian oscillator with *oscillatory*, long-lived memory around $\omega_0 \approx 0.1 \text{ eV}$. The

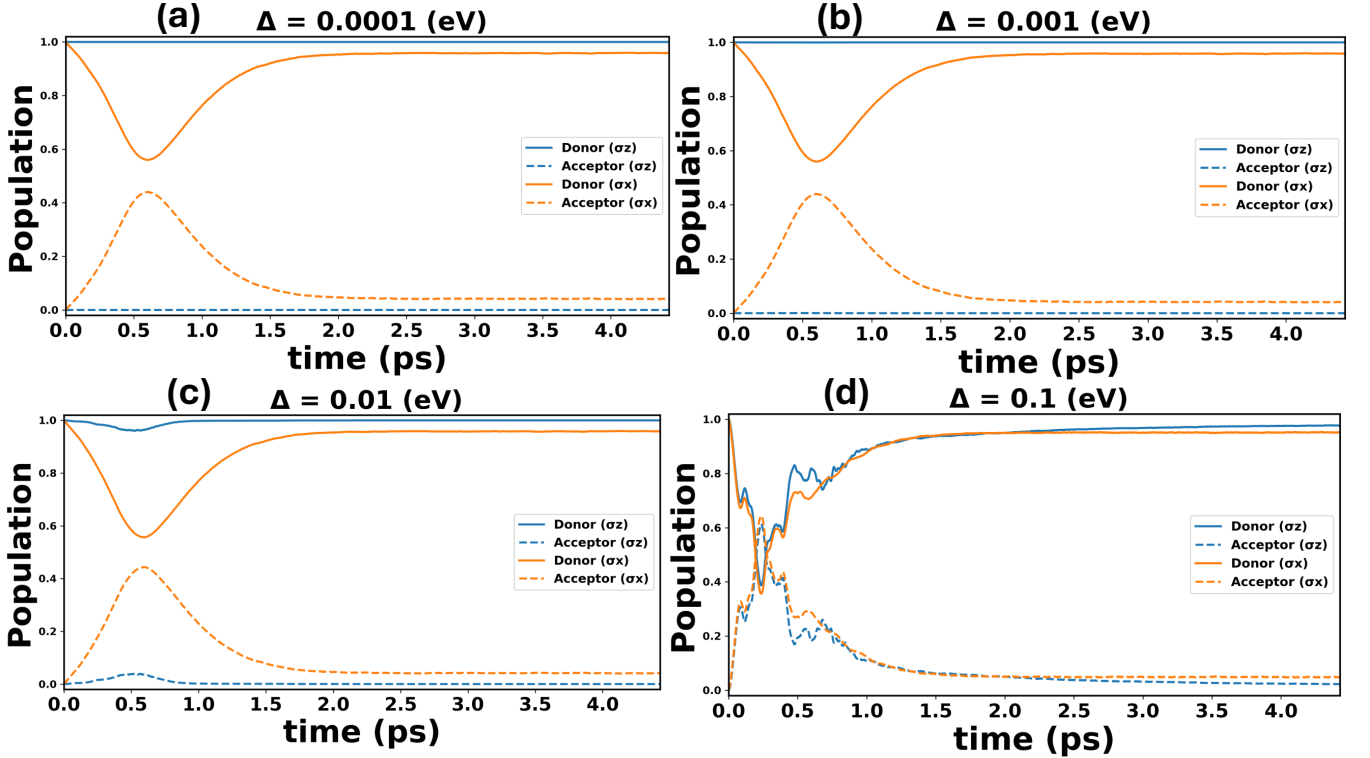


FIG. 3. **Population dynamics with a non-Markovian Ohmic bath: geometry (L) and electronic coupling (Δ) control coherence.** Dynamics are propagated with the non-Markovian SSE (NMSSE) using an Ohmic spectral density (Drude–Lorentz cutoff) with finite memory. Parameters (eV unless noted): $\epsilon = 0.1487$, $\omega_v = 0.1087$, $\Delta \in \{0.0001, 0.001, 0.01, 0.1\}$, $\alpha = 0.0005$, $\omega_c = 0.5$, $\gamma_E = 0.05$, $T = 0.025 \approx 290$ K. The bath reorganization is small, $\lambda_{\text{bath}} = \frac{1}{2}\alpha\omega_c = 1.25 \times 10^{-4}$ eV, so dynamics are dominated by system geometry. Curves show donor/acceptor populations for diagonal coupling $L = \gamma_E\sigma_z$ (solid/dashed blue) and off-diagonal coupling $L = \gamma_E\sigma_x$ (solid/dashed orange). (a) $\Delta = 0.0001$ eV. With $L = \gamma_E\sigma_z$ (pure dephasing), populations remain essentially frozen (donor ≈ 1 , acceptor ≈ 0). With $L = \gamma_E\sigma_x$, weak but clear coherent transfer occurs: a single underdamped swing moves population to the acceptor (~ 0.4) before relaxing back as memory-assisted damping sets in. (b) $\Delta = 0.001$ eV. The σ_z case stays static; σ_x shows a faster, larger excursion with smoother relaxation—coherence persists but damps within \sim ps due to finite bath memory at 290 K. (c) $\Delta = 0.01$ eV. Small oscillatory ripples now appear even for σ_z (Hamiltonian mixing by Δ leaks through despite dephasing). The σ_x channel exhibits pronounced coherent exchange followed by damping to a donor-dominated steady state. (d) $\Delta = 0.1$ eV. Strong early-time transients and visible oscillations occur for both $L = \gamma_E\sigma_z$ and $L = \gamma_E\sigma_x$, then relax toward a common quasi-steady population. The oscillation period shortens with Δ , consistent with an effective Rabi frequency increasing with Δ , while non-Markovian damping from the Ohmic kernel suppresses long-time coherence.

contrast reveals how memory *geometry* and *spectral selectivity* reshape population dynamics across the same Δ -sweep and system operators $L = \gamma_E\sigma_z$ (diagonal) vs $L = \gamma_E\sigma_x$ (off-diagonal).

With the Ohmic bath (Fig. 3), populations show weak, short-lived oscillations (coherence “fingerprints”) that are quickly damped at $T \approx 290$ K. In the structured bath (Fig. 4), the same Δ -sweep displays *clear beats* and underdamped oscillations during the first picosecond. This difference comes directly from the bath correlation function $C(t)$: Ohmic $C(t)$ decays monotonically, whereas the Structured $C(t)$ carries an oscillatory component at ω_0 , feeding phase information back into the system and sustaining coherence longer.

In Fig. 3 (Ohmic), late-time populations are donor-favored for σ_z across small and moderate Δ , and ap-

proach a common quasi-steady value for σ_x . In Fig. 4 (structured), σ_x robustly relaxes toward $\sim 1/2$ – $1/2$ across Δ (bath-assisted equilibration along the tunneling path), while σ_z exhibits a Δ -controlled crossover: donor-dominated at small Δ , then—by $\Delta = 0.1$ eV—*acceptor-favoring* due to resonant assistance from the environmental mode. Thus, the structured bath not only extends coherence but can *reroute* the final population balance in a geometry-dependent way.

In our model the Spike (mode near ω_v) and the ACE2 electronic gap ϵ couple to an environment. For the Ohmic case, ET is facilitated mainly by vibrational reorganization tuned by γ (Fig. 3): the bath helps briefly but does not sustain coherence; transfer efficiency is controlled by the balance of Δ and mild memory (ω_c^{-1}). For the structured case, the environmental mode near ω_0 gates ET:

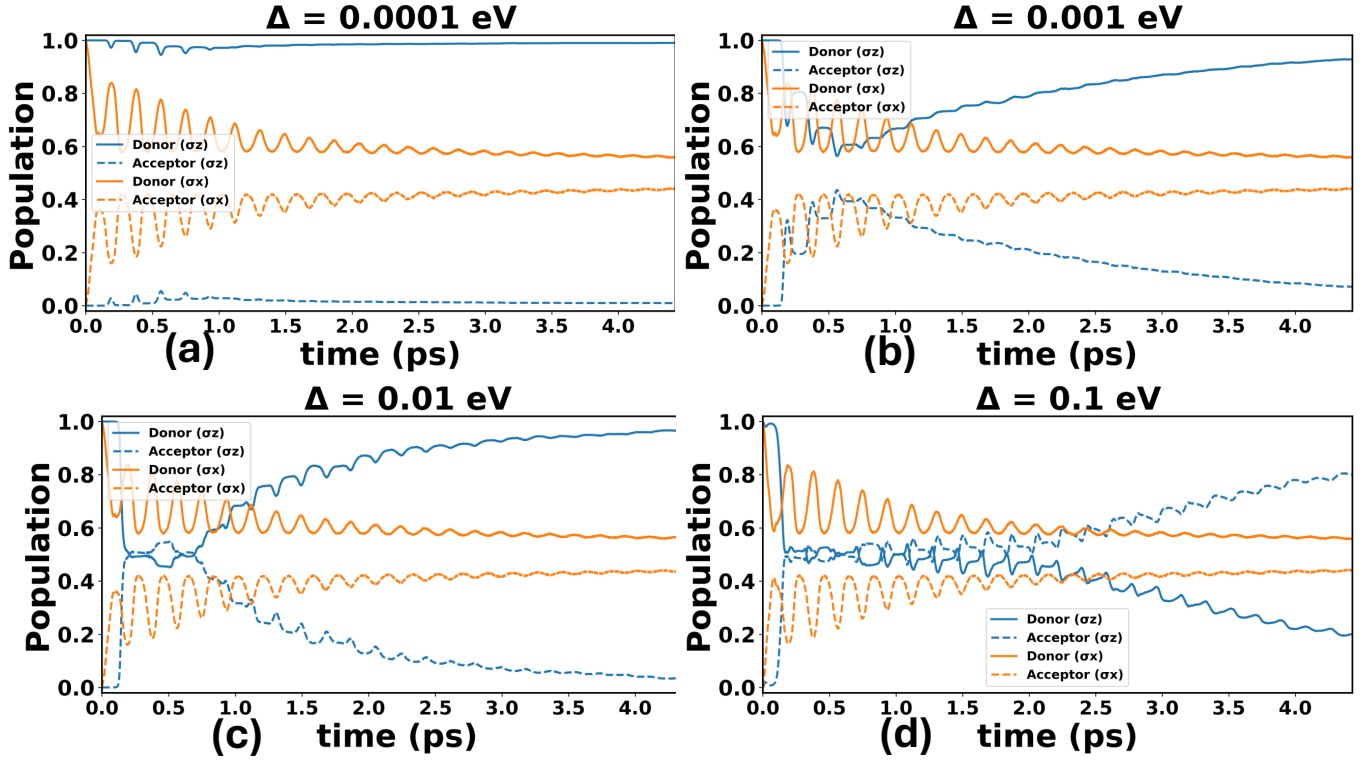


FIG. 4. **Population dynamics with a structured non-Markovian bath: Δ -controlled crossover and geometry selectivity.** Dynamics are propagated with the *non-Markovian SSE* (NMSSE) and an *underdamped Brownian* spectral density (structured bath). Parameters (eV unless noted): $\epsilon = 0.1487$, $\omega_v = 0.1487$, $\Delta \in \{0.0001, 0.001, 0.01, 0.1\}$; structured bath ($\omega_0 = 0.1$, $\beta = 0.005$, $\alpha = 0.08$); stochastic coupling $\gamma_E = 0.01$; $T = 0.025 \approx 290$ K. A narrow linewidth ($\beta = 0.005$) yields long-lived oscillatory correlations at $\omega_0 \simeq 0.1$ that imprint beats on the populations. Curves: donor/acceptor for diagonal coupling $L = \gamma_E \sigma_z$ (solid/dashed blue) and off-diagonal coupling $L = \gamma_E \sigma_x$ (solid/dashed orange). (a) $\Delta = 0.0001$ eV. The structured memory produces clear underdamped oscillations in both geometries during the first picosecond. With $L = \sigma_z$, dephasing plus memory-driven localization leaves the donor near ~ 0.7 at late times. With $L = \sigma_x$, the bath modulates the tunneling path, creating a larger initial swing and relaxation toward a near-balanced state. (b) $\Delta = 0.001$ eV. Increasing Δ strengthens Hamiltonian mixing. In σ_z , donor recovers steadily while acceptor drains; in σ_x , oscillations persist but damp to $\sim 0.5/0.5$ within a few ps. (c) $\Delta = 0.01$ eV. Memory-induced beats remain visible up to ~ 1.5 ps. The σ_z channel relaxes to a donor-dominated state ($\gtrsim 0.85$), whereas σ_x stays near equipartition ($\approx 0.5 \pm 0.05$). (d) $\Delta = 0.1$ eV. Strong coherent transients with pronounced beating appear in both geometries.

it transiently locks the ACE2 donor–acceptor superposition to its phase, producing beats that *enhance* mixing (especially for σ_x) and, for σ_z , can steer population toward the acceptor at larger Δ . Operationally, this means that in an ACE2–Spike setting, a narrow environmental feature (e.g., protein/solvent collective mode) can both *amplify* early-time coherent exchange and *bias* the late-time outcome—facilitating ET without requiring large reorganization energy.

Across both figures we work in an intermediate regime: the stochastic coupling γ_E is modest (Ohmic: 0.05; structured: 0.05) and temperature is room-like, so neither strong localization nor fully coherent unitary dynamics dominate. In this window, Δ and L determine how much of the environmental memory is *converted* into useful coherence vs damping.

Ohmic (Fig. 3). $C(t)$ decays quickly, so g_0 dominates: it damps and localizes. The g_1 (coherence

feedback) channel is present but short-lived; hence the modest early oscillations and donor-leaning late state under σ_z , with σ_x relaxing toward a mild quasi-equilibrium. *Structured* (Fig. 4). $C(t)$ contains an oscillatory part near ω_0 , so $g_1(t)$ remains sizable and *phase-coherent* over longer times: for $L = \gamma_E \sigma_x$ (where $[\sigma_x, H_{\text{sys}}] \propto \epsilon \sigma_y$), this directly drives coherent population exchange and then bath-assisted equilibration; for $L = \gamma_E \sigma_z$ (where $[\sigma_z, H_{\text{sys}}] \propto \Delta \sigma_y$), increasing Δ strengthens the coherence-feedback pathway, enabling the observed crossover to acceptor-favoring outcomes.

Moreover, a narrow, moderately coupled mode (structured bath) can *extend* coherence and *bias* final populations—useful for facilitating ET toward the acceptor state in ACE2 when Δ is not extremely small. The Off-diagonal coupling ($L = \gamma_E \sigma_x$) exploits the g_1 channel most efficiently, leading to robust early-time transfer and near-equipartition steady states; diagonal cou-

pling ($L = \gamma_E \sigma_z$) needs larger Δ to harvest the same memory for net acceptor gain. Compared with the non-Markovian Ohmic case (Fig. 3), the structured bath (Fig. 4) turns environmental memory from a passive damper into an *active control knob*: it amplifies early coherence (via g_1), shapes late-time populations (via geometry-dependent competition with g_0), and thereby *facilitates* ACE2-Spike electron transfer in regimes where purely Ohmic memory would yield weaker and more donor-biased outcomes.

Figure 5 (a,b) Population dynamics: (a) non-Markovian *structured* bath with $\gamma = 0$ (no Spike coupling) vs (b) *closed* system with $\gamma = 0.1$ (Spike coupled) but no bath. Panel (a) includes a *structured*, non-Markovian environment and uses the NMSSE; panel (b) removes the environment entirely ($\gamma_E = \alpha = 0$), leaving purely unitary dynamics with a finite Spike coupling γ . Strikingly, (a) shows noticeable population motion (orange, $L = \sigma_x$) and weak beats, despite $\gamma = 0$; (b) remains pinned at donor ≈ 1 even though $\gamma = 0.1$.

The NMSSE evolves the state with three ingredients: where the memory integral furnishes two effective contributions:

$$\underbrace{\gamma_E(L - \langle L \rangle_t) \zeta_t}_{\text{stochastic drive}} + \underbrace{g_0(t) \gamma_E^2 (\langle L \rangle_t L - \langle L \rangle_t^2)}_{\text{dissipative localization}} + \underbrace{g_1(t) \gamma_E^2 C[(H_{\text{sys}}, L)]}_{\text{coherence feedback}}$$

lier conundrum of low-frequency vibrational assistance: it is not that the Spike mode provides all the energy (which would be improbable for MHz frequencies), but rather that the Spike mode, by modulating the coupling pathways, allows the system to exploit environmental energy on a slow timescale. Essentially, the mode “turns on” the tunneling when conditions are right, by transiently forming an optimal tunneling configuration. This could, for instance, involve transient alignment of a conductive pathway (e.g., a chain of amino acids or water molecules bridging the donor and acceptor) which is synchronized with a specific motion of Spike. The result is an electron transfer that would otherwise be extremely unlikely (given the energy mismatch) becoming feasible. This quantum trigger could be the initiating factor for subsequent biochemical changes—for example, reduction of a disulfide bond in ACE2 that then causes a large conformational shift, securing the virus-receptor binding. While speculative, this scenario aligns with the sharp on/off behavior and selectivity enhancement that our model exhibits when both vibrational assistance and non-Condon effects are present^{22,23}.

D. Optimization of the vibrational molecular switch

- For $\mathbf{L} = \gamma_E \sigma_z$ (blue): with $\Delta = 10^{-4}$ eV, $[\sigma_z, H_{\text{sys}}] \propto \Delta \sigma_y$ is tiny, so the \mathbf{g}_1 channel is negligible; g_0 then *localizes* populations—flat donor/acceptor curves.

- For $\mathbf{L} = \gamma_E \sigma_x$ (orange): $[\sigma_x, H_{\text{sys}}] \propto \epsilon \sigma_y$ is large, so \mathbf{g}_1 is *active*. The structured correlation $C(t)$ oscillates at $\omega_0 = 0.1$ with long memory ($\tau_c \sim 0.83$ ps), producing the observed *underdamped beats* during the first few hundred femtoseconds. As time grows, \mathbf{g}_0 integrates the colored noise and motionally-narrows the dynamics, relaxing the system toward a *near-equipartition* steady state along the tunneling channel—even though $\gamma = 0$.

With $\gamma_E = \alpha = 0$ the NMSSE reduces to $-iH_{\text{sys}}$ (no noise, no memory). The longitudinal Spike coupling $\gamma = 0.1$ dresses the TLS (polaron) and *reduces* tunneling: $\Delta_{\text{eff}} \approx \Delta e^{-2(\gamma/\omega_v)^2} \approx 4.0 \times 10^{-5}$ eV. Because $\epsilon \gg \Delta_{\text{eff}}$, the maximum unitary acceptor population is $\sim 7 \times 10^{-8}$ —far below plot resolution—so both “ σ_z ” and “ σ_x ” traces appear flat. Any tiny Rabi ripples occur at $\Omega \approx \epsilon/\hbar$ (period ~ 28 fs) but with vanishing amplitude.

Panel (a) shows that a *structured*, weakly coupled environment can *assist* electron transfer in the ACE2-Spike model even when the explicit Spike vibrational coupling is off ($\gamma = 0$): the stochastic drive plus coherence-feedback (g_1) transiently amplify mixing for $L = \gamma_E \sigma_x$ and steer the system toward a balanced population. By contrast, **Panel (b)** shows that, in the *absence* of environmental channels, a sizable Spike coupling ($\gamma = 0.1$) at small Δ merely *dresses* the TLS and suppresses tunneling (polaronic narrowing), leaving the system bias-locked on the donor.

For the ACE2-Spike system, the inclusion of non-Condon coupling provides a plausible solution to the ear-

Bringing together the insights from the above results, we can delineate the conditions for optimal performance of the ACE2-Spike ET switch in terms of sensitivity (high contrast between presence and absence of Spike vibration) and selectivity (ability to discriminate the correct vibrational frequency of Spike vs a slightly different one). The key ingredients for optimal behavior are:

- 1. Resonant vibrational coupling:** The mode frequency ω_v should match or slightly offset the donor-acceptor bias (including any renormalization by the environment). This maximizes the resonant energy exchange. In practice, ω_v around a few meV (terahertz frequency) is plausible for Spike^{26,27} and could resonate with typical redox gaps (which are often on the order of 0.1 eV when aided by reorganization energy)³³.
- 2. Strong non-Condon Effect:** A off-diagonal coupling modulate the dynamics effectively and incorporating the nuclear motion of spike-protien enhancing the ET mechanism compared to diagonal coupling. Our simulations suggest that an ET regime in olfactory receptors σ_x outperformed σ_z yields the best switch characteristics^{30,36}.
- 3. Structured environment (non-Markovian noise):** The bath should have a dominant low-frequency component (sub-Ohmic) to prolong coherence and allow the vibrational gating to manifest. An environment that is too fast (Ohmic) will continuously jostle the system and smear out the vibrational effects. In contrast, a slower environment

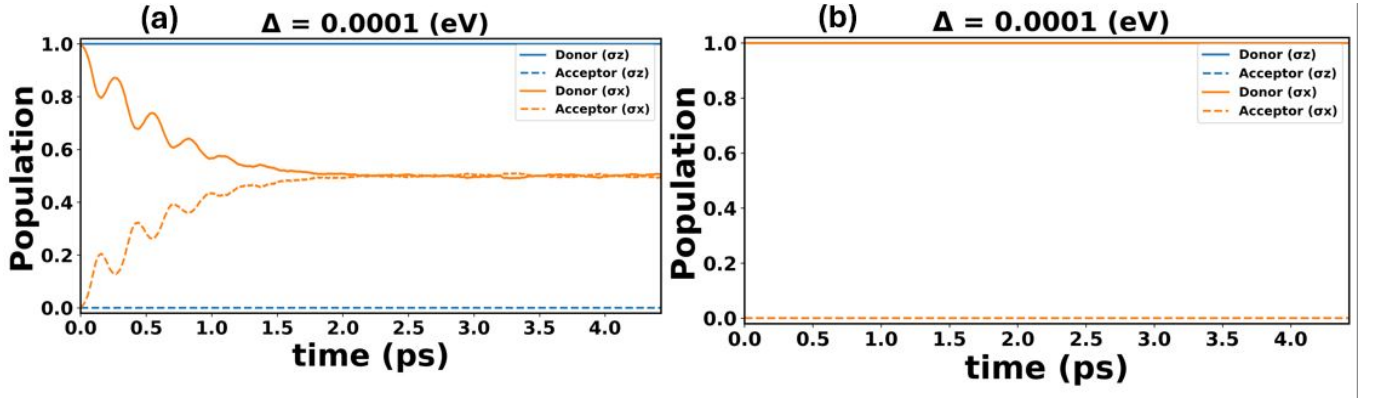


FIG. 5. Population dynamics: (a) non-Markovian *structured bath* with $\gamma = 0$ (no Spike coupling) vs (b) *closed system* with $\gamma = 0.1$ (Spike coupled) but no bath. Common parameters (eV unless noted): $\epsilon = 0.1487$, $\Delta = 10^{-4}$, $\omega_v = 0.1487$, $T = 290$ K. Time grid: $t \in [0, 1000]$ with $dt = 0.10$ (window 4.427 ps, step 0.443 fs). (a) **Structured non-Markovian bath (UBO):** $\omega_0 = 0.1$, $\beta = 0.005$, $\alpha = 0.08$, $\gamma_E = 0.01$, $M = 512$. Bath correlation is oscillatory, with period $T_0 \simeq 4.14/\omega_0 \approx 41$ fs and memory time $\tau_c \simeq \hbar/\beta \approx 830$ fs. $\gamma = 0 \Rightarrow \lambda_{\text{mode}} = 0$. (b) **Closed spin–boson limit:** $\gamma_E = 0$, $\alpha = 0 \Rightarrow$ no stochastic drive or memory kernels (plain Schrödinger dynamics). Spike–mode coupling on: $\gamma = 0.1 \Rightarrow \lambda_{\text{mode}} = 2\gamma^2/\omega_v \approx 0.1345$ eV. Polaron narrowing of tunneling: $\Delta_{\text{eff}} \approx \Delta e^{-2(\gamma/\omega_v)^2} \approx 4.0 \times 10^{-5}$ eV. The bias strongly dominates: maximal unitary transfer $P_A^{\text{max}} \approx (\Delta_{\text{eff}}/\sqrt{\epsilon^2 + \Delta_{\text{eff}}^2})^2 \sim 7 \times 10^{-8}$ (visually flat).

effectively filters out high-frequency noise, which not only protects coherence but also means the system-bath exchange is happening on timescales closer to the vibrational period—making it easier to synchronize with the Spike mode.^{31,32,62}

In the case of ACE2 and Spike the idea that the wild-type Spike protein might have the right vibrational modes to trigger ACE2, whereas perhaps certain mutations or modifications (or even a different coronavirus’s Spike) might not, thereby influencing infectivity²¹. This is admittedly speculative at this stage, but our quantitative model provides a framework for such hypotheses.

V. CONCLUSIONS

We have presented a detailed quantum dynamical study of vibrationally-assisted electron transfer in the ACE2–Spike protein complex, treating it as an open quantum system with both diagonal and off-diagonal system–environment interactions. By leveraging the non-Markovian quantum state diffusion formalism, we were able to simulate regimes that lie beyond the validity of conventional perturbative or semiclassical approaches. Our findings demonstrate several key points:

(1) In the appropriate limit (fast-relaxing Ohmic environment, high temperature, weak non-Condon coupling), our model reproduces classical Marcus–Jortner ET behavior. This served to validate the modeling and numerics. However, we also found that even moderate deviations from this limit (lower T , larger Δ , etc.) result in deviations from simple exponential kinetics and quantitative differences from Marcus rate predictions, underlining the necessity of a quantum approach for accuracy in less

classical regimes^{6,42}.

(2) The structured, sub-Ohmic environment typical of a protein–membrane setting exerts a significant influence on ET dynamics. Unlike a memoryless bath, the non-Markovian bath preserves quantum coherence over longer times and induces a slow-decaying component in the dynamics. While this can slow down the overall transfer rate (due to transient localization), it also provides a mechanism to sharpen the response of the system to resonant driving. The environment’s memory effectively creates a filtering effect that is beneficial for frequency-selective processes^{31,32,62}.

(3) The inclusion of non-Condon (off-diagonal) coupling is essential to capture the full scope of the VA-ET mechanism. Non-Condon effects allow the vibrational mode of the Spike protein to modulate the electron tunneling pathway in a time-dependent manner. This leads to inelastic tunneling processes whereby environmental fluctuations can cooperate with the vibrational mode to facilitate electron jumps that would be highly suppressed under purely diagonal coupling. We showed that even a moderate off-diagonal coupling qualitatively changes the system’s behavior, introducing rapid initial transfer, non-exponential kinetics, and a pronounced frequency selectivity to the vibrational assistance. In short, the non-Condon coupling turns the system into a much more finely tuned detector of the vibrational mode^{29,30,36}.

(4) Considering the ACE2–Spike complex as a prototype, our results lend theoretical support to the idea that quantum mechanical processes might play a functional role in viral infection mechanisms^{22,23}. If the Spike protein’s binding indeed induces an electron transfer in ACE2 (for example, reducing a disulfide bond), then the rate and likelihood of that ET could be crucial in deter-

mining whether the binding leads to successful cell entry. Our model suggests that evolution could have optimized this process: Spike's vibrational dynamics and the receptor's environment may be coadapted to maximize the chance of electron transfer, thus "locking" the spike onto the cell. This goes beyond the classic static lock-and-key picture by adding a dynamic, frequency-dependent lock^{20,21,63}.

(5) From a practical standpoint, these insights hint at new avenues for intervention. If a particular vibrational mode of Spike is critical for promoting the electron transfer and subsequent viral entry, disrupting that mode could reduce infectivity. This could be achieved by small molecules that bind to Spike and alter its stiffness or vibrational spectrum, or by external physical means (e.g., terahertz irradiation tuned to those modes²⁸), though delivering that in vivo is nontrivial. Alternatively, targeting the ACE2 environment to either dampen the necessary environmental fluctuations or conversely to introduce mismatched fluctuations might diminish the efficiency of the VA-ET switch. In the language of our model, one could aim to detune the resonance condition or to diminish the off-diagonal coupling pathway^{30,33}.

Looking forward, there are several exciting directions to extend this research. One important generalization is to include multiple vibrational modes of the Spike protein. The Spike is a large structure with a rich vibrational spectrum; multiple modes could conceivably contribute to or compete in assisting the ET. A multimode quantum simulation (while more computationally intensive) could reveal interference effects between modes and whether a broad spectrum vs a single mode matters for the efficiency. It would also allow us to assess robustness: if one mode's frequency is slightly off, could another mode still activate the switch, providing redundancy^{26,27}?

Another direction is to refine the environmental model by drawing on atomistic molecular dynamics (MD) simulations of the ACE2–Spike complex embedded in a membrane⁶⁴. By analyzing MD trajectories, one could extract a more realistic spectral density $J(\omega)$ (including perhaps specific vibrational peaks corresponding to protein motions and membrane collective modes). This data-driven spectral density could replace our idealized sub-Ohmic form and improve quantitative accuracy, ensuring that our values correspond to physically observed fluctuations. It would also be interesting to incorporate the effect of the membrane's electric field fluctuations, which have been suggested to affect Spike behavior²⁸.

In conclusion, the quantum model developed in this work provides a window into how vibrational motions and complex environmental fluctuations can conspire to influence electron transfer in a biological receptor. The ACE2–Spike system, while motivated by a pressing biomedical problem, also serves as a case study for a broader class of phenomena where a biochemical "switch" might be regulated by quantum dynamics. Our findings underscore that capturing such phenomena requires going beyond traditional theories and embracing the full

richness of open quantum systems theory. They also provoke new questions about the prevalence of such mechanisms in biology and how one might harness or disrupt them for technological and therapeutic ends.

Appendix A: Equations of Motion for Stochastic Schrödinger Dynamics

This appendix provides the equations of motion derived from the (EQ. 16)

1. Markovian Limit (White Noise)

In the Markovian limit, the environmental correlation time approaches zero, reducing the dynamics to white noise. The equation of motion simplifies to:

$$\frac{d}{dt}|\tilde{\psi}_z(t)\rangle = -iH_{\text{sys}}|\tilde{\psi}_z(t)\rangle + \gamma_E(L - \langle L \rangle_t)|\tilde{\psi}_z(t)\rangle\tilde{z}_t - \frac{\gamma_E^2}{2}(L^\dagger L - 2\langle L^\dagger \rangle_t L + \langle L^\dagger \rangle_t^2)|\tilde{\psi}_z(t)\rangle \quad (\text{A1})$$

The stochastic Schrödinger equation in the Markovian limit simplifies to:

$$\frac{d}{dt}|\tilde{\psi}_z(t)\rangle = -iH_{\text{sys}}|\tilde{\psi}_z(t)\rangle + \gamma_E(\sigma_z - \langle \sigma_z \rangle_t)|\tilde{\psi}_z(t)\rangle\tilde{z}_t - \frac{\gamma_E^2}{2}(\sigma_z^2 - 2\langle \sigma_z \rangle_t \sigma_z + \langle \sigma_z \rangle_t^2)|\tilde{\psi}_z(t)\rangle \quad (\text{A2})$$

where \tilde{z}_t is real Gaussian white noise. The stochastic term $\gamma_E(\sigma_z - \langle \sigma_z \rangle_t)|\tilde{\psi}_z(t)\rangle\tilde{z}_t$ drives energy bias fluctuations that enable thermal activation over barriers, while the dissipative term $-\frac{\gamma_E^2}{2}(\sigma_z^2 - 2\langle \sigma_z \rangle_t \sigma_z + \langle \sigma_z \rangle_t^2)|\tilde{\psi}_z(t)\rangle$ suppresses these fluctuations toward the mean value $\langle \sigma_z \rangle_t$. In the Markovian limit, the absence of memory kernels ($g_0(t)$, $g_1(t)$) eliminates non-Markovian feedback, resulting in purely diffusive dynamics along the energy bias coordinate.

2. Non-Markovian Case: Diagonal Coupling ($L = \gamma_E \sigma_z$)

For diagonal coupling with $L = \gamma_E \sigma_z$, the equation of motion including first-order non-Markovian corrections is:

$$\begin{aligned} \frac{d}{dt}|\tilde{\psi}_z(t)\rangle = & -iH_{\text{sys}}|\tilde{\psi}_z(t)\rangle + \gamma_E(\sigma_z - \langle \sigma_z \rangle_t)|\tilde{\psi}_z(t)\rangle\tilde{z}_t \\ & + g_0(t)\gamma_E^2(\langle \sigma_z \rangle_t \sigma_z - \langle \sigma_z \rangle_t^2)|\tilde{\psi}_z(t)\rangle \\ & + ig_1(t)\gamma_E^2\Delta[(\sigma_x + i\langle \sigma_z \rangle_t \sigma_y) - \langle \sigma_x + i\langle \sigma_z \rangle_t \sigma_y \rangle_t]|\tilde{\psi}_z(t)\rangle \end{aligned} \quad (\text{A3})$$

3. Non-Markovian Case: Off-Diagonal Coupling ($L = \gamma_E \sigma_x$)

For off-diagonal coupling with $L = \gamma_E \sigma_x$, the equation of motion is:

$$\begin{aligned} \frac{d}{dt} |\tilde{\psi}_z(t)\rangle &= -iH_{\text{sys}} |\tilde{\psi}_z(t)\rangle + \gamma_E (\sigma_x - \langle \sigma_x \rangle_t) |\tilde{\psi}_z(t)\rangle \tilde{z}_t \\ &+ g_0(t) \gamma_E^2 (\langle \sigma_x \rangle_t \sigma_x - \langle \sigma_x \rangle_t^2) \psi_t \\ &- i g_1(t) \gamma_E^2 [\epsilon (\sigma_z - \langle \sigma_z \rangle_t) + 2\gamma (\sigma_z x - \langle \sigma_z x \rangle_t)] |\tilde{\psi}_z(t)\rangle \end{aligned} \quad (\text{A4})$$

The time-dependent kernels $g_0(t)$ and $g_1(t)$ are determined by the environmental correlation function $C(t, s)$ as defined in Eqs. (16)-(17) of the main text.

ACKNOWLEDGMENTS

This work was funded by United Arab Emirates University Research Affairs under Grant number G-00003550.

CONFLICT OF INTEREST

The authors have no conflicts to disclose.

AUTHOR CONTRIBUTIONS STATEMENT

Muhammad Waqas Haseeb and Mohammad Toutounji contributed equally to the research presented in this manuscript. Muhammad Waqas Haseeb, as the first author, was responsible for drafting the initial manuscript and conducting the core calculations and data analysis under the supervision of Mohammad Toutounji. Professor Toutounji played a central role in developing the conceptual framework of the study, providing critical insights and ongoing guidance throughout both the research and manuscript preparation phases. He also undertook a thorough review and refinement of the manuscript to ensure scientific clarity and rigor. Both authors have reviewed and approved the final version of the manuscript for publication.

DATA AVAILABILITY

The research data and parameters referenced in this study are well-documented in the associated published papers. All figures-source data and scripts that generated them are available at [\[GitHub https://github.com/waqashaseeb\]](https://github.com/waqashaseeb).

¹M. Mohseni, Y. Omar, G. S. Engel, and M. B. Plenio, *Quantum Effects in Biology* (Cambridge University Press, 2014).

²H. B. Gray and J. R. Winkler, *Quarterly Reviews of Biophysics* **36**, 341 (2003).

³C. C. Moser, J. L. R. Anderson, and P. L. Dutton, *Biochimica et Biophysica Acta (BBA) - Bioenergetics* **1797**, 1573 (2010).

⁴J. O. Richardson, *The Journal of Physical Chemistry Letters* **15**, 7387 (2024).

⁵E. R. Heller and J. O. Richardson, *The Journal of Chemical Physics* **152** (2020).

⁶H.-P. Breuer and F. Petruccione, *The Theory of Open Quantum Systems* (Oxford University Press, 2002).

⁷D. Gribben, A. Strathearn, J. Iles-Smith, D. Kilda, A. Nazir, B. W. Lovett, and P. Kirton, *Physical Review Research* **2**, 013265 (2020).

⁸N. May and O. Kühn, *Charge and Energy Transfer Dynamics in Molecular Systems* (John Wiley & Sons, 2023).

⁹G. S. Engel, T. R. Calhoun, E. L. Read, T.-K. Ahn, T. Mančal, Y.-C. Cheng, R. E. Blankenship, and G. R. Fleming, *Nature* **446**, 782 (2007).

¹⁰T. Brixner, J. Stenger, H. M. Vaswani, M. Cho, R. E. Blankenship, and G. R. Fleming, *Nature* **434**, 625 (2005).

¹¹R. van Grondelle and V. I. Novoderezhkin, *Procedia Chemistry* **3**, 198 (2011).

¹²T. Kondo, W. J. Chen, and G. S. Schulau-Cohen, *Chemical Reviews* **117**, 860 (2017).

¹³J. P. Bothma, J. B. Gilmore, and R. H. McKenzie, *New Journal of Physics* **12**, 055002 (2010).

¹⁴D. De Vault and B. Chance, *Biophysical Journal* **6**, 825 (1966).

¹⁵L. Turin, *Chemical Senses* **21**, 773 (1996).

¹⁶J. C. Brookes, F. Hartoutsiou, A. P. Horsfield, and A. M. Stoneham, *Physical Review Letters* **98**, 038101 (2007).

¹⁷L. Turin, *Chemical Senses* **21**, 773 (1996).

¹⁸E. R. Bittner, A. Madalan, A. Czader, and G. Roman, *The Journal of Chemical Physics* **137** (2012).

¹⁹S. Belouzard, J. K. Millet, B. N. Licitra, and G. R. Whittaker, *Viruses* **4**, 1011 (2012).

²⁰M. Hoffmann, H. Kleine-Weber, S. Schroeder, N. Krüger, T. Herrler, S. Erichsen, T. S. Schiergens, G. Herrler, N.-H. Wu, A. Nitsche, *et al.*, *Cell* **181**, 271 (2020).

²¹J. Lan, J. Ge, J. Yu, S. Shan, H. Zhou, S. Fan, Q. Zhang, X. Shi, Q. Wang, L. Zhang, *et al.*, *Nature* **581**, 215 (2020).

²²B. Adams, I. Sinayskiy, R. van Grondelle, and F. Petruccione, *Scientific Reports* **12**, 16929 (2022).

²³M. W. Haseeb and M. Toutounji, *Scientific Reports* **14** (2024).

²⁴S. Hati and S. Bhattacharyya, *ACS Omega* **5**, 16292 (2020).

²⁵J. Singh, R. S. Dhindsa, V. Misra, and B. Singh, *Computational and Structural Biotechnology Journal* **18**, 3705 (2020).

²⁶U. Author, “Effect of receptors on the resonant and transient harmonic vibrations of coronavirus,” (2021), *scientific Reports (PMC)*.

²⁷J. Yao and H. C. Wang, *Journal of Medical Virology* **92**, 2577 (2020).

²⁸U. Author, “Electromagnetic waves destabilize the sars-cov-2 spike protein and reduce sc2-vlp infectivity,” (2024), *nature Communications (PMC)*.

²⁹A. Milischuk and D. V. Matyushov, *The Journal of Physical Chemistry B* **111**, 4685 (2007).

³⁰U. Author, “Protein dynamics and electron transfer: Electronic decoherence and non-condon effects,” (2005), *PubMed record*; use the PubMed page to fill full bibliographic details if needed.

³¹E. Paladino, Y. M. Galperin, G. Falci, and B. L. Altshuler, *Reviews of Modern Physics* **86**, 361 (2014).

³²U. Author, “Aging power spectrum of membrane protein transport and other subordinated random walks,” (2021), *pMC article*.

³³U. Author, “Fluctuations in biological and bioinspired electron-transfer,” (2010), *pMC article*.

³⁴A. G. Redfield, in *Advances in Magnetic and Optical Resonance*, Vol. 1 (Elsevier, 1965) pp. 1–32.

³⁵D. Manzano, *AIP Advances* **10**, 025106 (2020).

³⁶M. Dixit *et al.*, *Physical Review B* **105**, 214310 (2022).

³⁷M. Dixit *et al.*, *Physical Review B* **105**, 214310 (2022).

³⁸J. Gilmore and R. H. McKenzie, *Journal of Physics: Condensed Matter* **17**, 1735 (2005).

³⁹Q. Shi, L.-P. Chen, Z. An, G. Nan, and Y. Zhao, *The Journal of Chemical Physics* **130**, 084505 (2009).

⁴⁰L. Diósi and W. T. Strunz, *Physics Letters A* **235**, 569 (1997).

⁴¹W. T. Strunz, L. Diósi, and N. Gisin, *Physical Review A* **61**, 022106 (1999).

⁴²S. Mukamel, *Principles of Nonlinear Optical Spectroscopy* (Oxford University Press, 1995).

⁴³Y. Tanimura, *The Journal of Chemical Physics* **153**, 020901 (2020).

⁴⁴L. Bouten, M. Guta, and H. Maassen, *Journal of Physics A: Mathematical and General* **37**, 3189 (2004).

⁴⁵R. Hartmann and W. T. Strunz, *Journal of Chemical Theory and Computation* **13**, 5834 (2017).

⁴⁶C.-Y. Hsieh and J. Cao, *The Journal of Chemical Physics* **148**, 014103 (2018).

⁴⁷W. T. Strunz, L. Diósi, and N. Gisin, *Physical Review Letters* **82**, 1801 (1999).

⁴⁸N. Makri and E. Sim, *The Journal of Chemical Physics* **109**, 9259 (1998).

⁴⁹Y. Tanimura and R. Kubo, *Journal of the Physical Society of Japan* **58**, 101 (1989).

⁵⁰A. Checińska, F. A. Pollock, L. Heaney, and A. Nazir, *The Journal of Chemical Physics* **142**, 01B609 (2015).

⁵¹A. Pavlova, Z. Zhang, A. Acharya, D. L. Lynch, Y. T. Pang, Z. Mou, J. M. Parks, C. Chipot, and J. C. Gumbart, *The Journal of Physical Chemistry Letters* **12**, 5494 (2021).

⁵²L. Casalino, Z. Gaieb, J. A. Goldsmith, C. K. Hjorth, A. C. Dommer, A. M. Harbison, C. A. Fogarty, E. P. Barros, B. C. Taylor, J. S. McLellan, E. Fadda, and R. E. Amaro, *ACS Central Science* **6**, 1722 (2020).

⁵³D. Wrapp, N. Wang, K. S. Corbett, J. A. Goldsmith, C.-L. Hsieh, O. Abiona, B. S. Graham, and J. S. McLellan, *Science* **367**, 1260 (2020).

⁵⁴I. A. Solov'yov, P.-Y. Chang, and K. Schulten, *Physical Chemistry Chemical Physics* **14**, 13861 (2012).

⁵⁵T. Mancini, N. Luchetti, S. Macis, V. Minicozzi, R. Mosetti, A. Nucara, S. Lupi, and A. D'Arco, *International Journal of Molecular Sciences* **26**, 10342 (2025).

⁵⁶G. Pezzotti, E. Ohgitani, Y. Fujita, H. Imamura, F. Pappone, A. Grillo, M. Nakashio, M. Shin-Ya, T. Adachi, T. Yamamoto, *et al.*, *ACS Infectious Diseases* **9**, 2226 (2023).

⁵⁷A. Santamaria, K. C. Batchu, O. Matsarskaia, S. F. Prévost, D. Russo, F. Natali, T. Seydel, I. Hoffmann, V. Laux, M. Haertlein, *et al.*, *Journal of the American Chemical Society* **144**, 2968 (2022).

⁵⁸Z. Kuang, J. Luginsland, C.-S. Hung, B. W. Stamps, R. J. Thomas, N. Kelley-Loughnane, O. N. Ruiz, and W. P. Roach, *Scientific Reports* **15**, 43920 (2025).

⁵⁹C. A. de March, N. Ma, C. B. Billesbølle, J. Tewari, C. Llinas del Torrent, W. J. C. van der Velden, I. Ojiro, I. Takayama, B. Faust, L. Li, *et al.*, *Nature* **635**, 499 (2024).

⁶⁰A. Marais, I. Sinayskiy, A. Kay, F. Petruccione, and A. Ekert, *New Journal of Physics* **15**, 013038 (2013).

⁶¹V. So, M. Duraisamy Suganthi, A. Menon, M. Zhu, R. Zhuravel, H. Pu, P. G. Wolynes, J. N. Onuchic, and G. Pagano, *Science Advances* **10**, eads8011 (2024).

⁶²U. Author, “Non-markovian dynamics of a dissipative two-level system: Nonzero bias and sub-ohmic bath,” (2009), aPS link.

⁶³S. Belouzard, J. K. Millet, B. N. Licitra, and G. R. Whittaker, *Viruses* **4**, 1011 (2012).

⁶⁴D. Di Tommaso, T. Fuksman, M. Reuter, E. Tuleu, D. P. Tielemans, and M. Orozco, *The Journal of Physical Chemistry B* **110**, 24546 (2006).